Earth, Planets and Space

EXPRESS LETTER

Open Access

Laboratory measurements show temperature-dependent permittivity of lunar regolith simulants

M. Kobayashi[1], H. Miyamoto[2,3*], B. D. Pál[4,5], T. Niihara[6] and T. Takemura[7]

Abstract

The mapping of available water–ice is a crucial step in the lunar exploration missions. Ground penetrating radars have the potential to map the subsurface structure and the existence of water–ice in terms of the electromagnetic properties, specifically, the permittivity. Slight differences in permittivity can be significantly important when applied in a dry environment, such as on the Moon and Mars. The capability of detecting a small fraction of putative water–ice depends on the permittivity changes in terms of its dependent parameters, such as the frequency, the temperature, the porosity, and the chemical composition. Our work aims at mitigating false detection or overlooking of water–ce by considering their conditions that previous researches did not cover. We measured the permittivity of different lunar regolith relevant analogue samples with a fixed 40 % porosity in the ultra-high-frequency–super-high-frequency band. We used the coaxial probe method to measure anorthosite, basalt, dunite and ilmenite at 20 °C, −20 °C and −60 °C, and we find that, at −60 °C, the permittivity decreases about 6–18 % compared with the values at 20 °C. Within this temperature range, the permittivity is quite similar to the permittivity of water–ice. We find that the conventional calculation would overestimate the permittivity in the low temperature areas, such as the permanently shadowed regions. We also find that each component in the lunar regolith has different temperature-dependent permittivity, which might be important for radar data analysis to detect lunar polar water–ice. Our results also suggest that it should be possible to estimate the water–ice content from radar measurements at different temperatures given an appropriate method.

Keywords Moon, Water–ice, Permittivity, Radar, Ground Penetrating Radar, Lunar mission, Lunar regolith

*Correspondence:
H. Miyamoto
hm@sys.t.u-tokyo.ac.jp
Full list of author information is available at the end of the article

Graphical Abstract

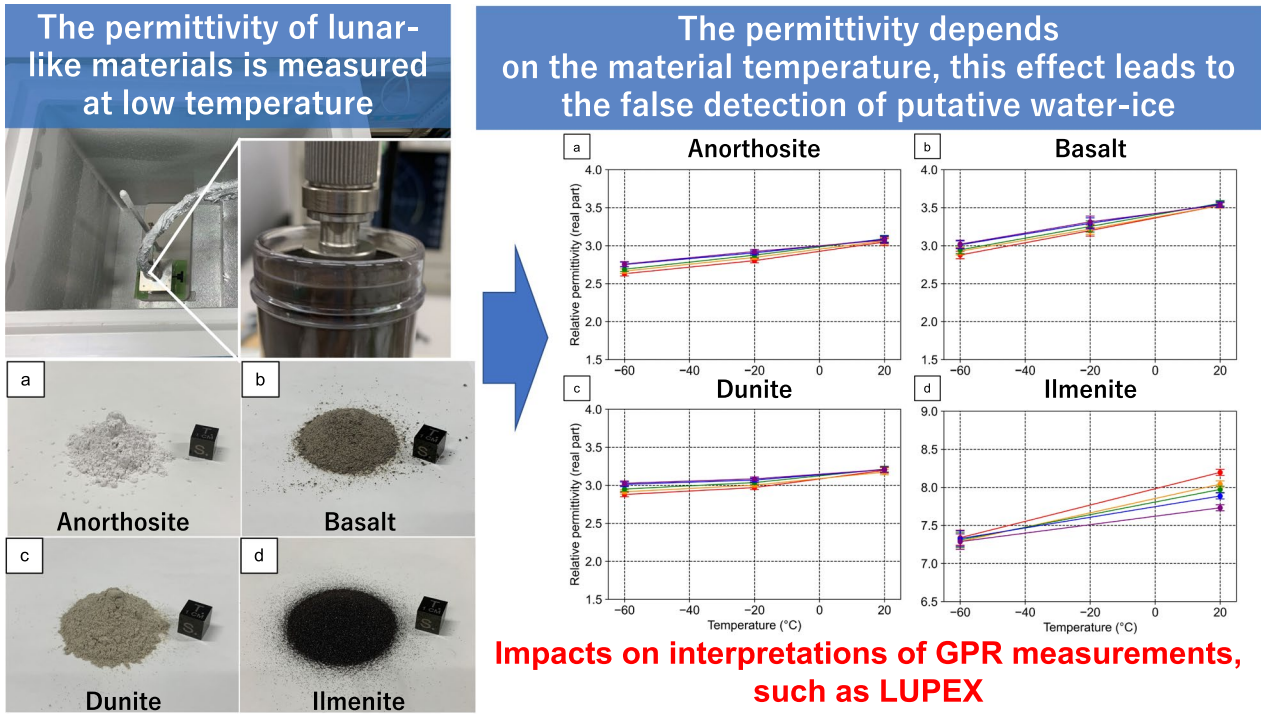

Introduction

The existence of putative water–ice on the Moon has been a frequently debated topic for the last decades (Arnold 1979; Watson et al. 1961). Multiple observations have implied the existence of water–ice, especially in the low-temperature regions of the lunar poles in permanently shadowed regions (Colaprete et al. 2010; Feldman et al. 1998; Lawrence et al. 2006; Li et al. 2018; Nozette et al. 1996; Spudis et al. 2013; Zuber et al. 2012; Kereszturi 2020). The water–ice on the Moon has substantial scientific values and is also a vital resource for future explorations and long-term missions on the Moon. However, there is no consensus about the amount and distribution of water–ice. The estimated amount in the regolith ranges from less than 1.0 wt% (Miller et al. 2012; Pieters et al. 2009; Sanin et al. 2017) to about 30 wt% (Li et al. 2018). Moreover, the estimated distribution by different observations does not match (e.g., Fisher et al. 2017; Hayne et al. 2015; Li et al. 2018). Thus, several landing missions such as Lunar Polar Exploration (LUPEX), Volatiles Investigating Polar Exploration Rover (VIPER), and Chang'E-6 aim at gathering data about the amount and distribution of water–ice in the lunar polar region (Colaprete et al. 2019; Hoshino et al. 2020). The existence of ice could be examined through in-situ analysis of subsurface materials by drilling, which is technically possible up to a few meters (Boazman et al. 2022). In our work, we focus on obtaining information about the subsurface up to this depth and aid the selection of candidate sites.

One observational instrument that can obtain information on the lunar subsurface up to a few meters in depth and with a high resolution is the Ground-Penetrating Radar (GPR). GPRs use high-frequency radio waves to image the subsurface. Electromagnetic (EM) waves reflect or scatter at the boundary between materials with different dielectric properties. The behavior of EM waves in a medium is mainly determined by permittivity, permeability, and conductivity. For the Apollo samples, the conductivity is typically almost zero ($10^{-9} - 10^{-14}$ S/m) (Heiken et al. 1991), which means that the maximum attenuation rate is in the order of 10^{-7} dB/m in the lunar regolith and can be negligible for the EM propagation through the lunar regolith. In GPRs frequency range, most minerals (except for magnetic minerals) have no ferromagnetism, so the permeability is almost the same as the magnetic constant (permeability in vacuum), and does not affect the propagation of EM waves through soils or rocks (Martinez and Byrnes 2001). Thus, permittivity is the only dominant parameter for EM propagation

through lunar regolith. This physical exploration method has been conducted by the previous Chang'E missions (Xiao et al. 2015; Li et al. 2020; Zhang et al. 2020). LUPEX is also equipped with a GPR to identify regolith structures before drilling.

In-situ observations have been conducted to estimate lunar regolith permittivity (e.g., Dong et al. 2017, 2021; Ishiyama et al. 2013; Su et al. 2022), but the accuracy is limited, which makes laboratory measurements to be one of the best methods to estimate permittivity. A reliable data set was compiled from the Apollo missions measured under dry conditions at various temperatures (e.g., Chung and Westphal 1973; Frisillo et al. 1975; Gold et al. 1976; Olhoeft and Strangway 1975; Heiken et al. 1991). The relative permittivity is associated with the bulk density and $FeO+TiO_2$ content (e.g., Heiken et al. 1991; Olhoeft and Strangway 1975), and more recent results came from the JSC-1A (Johnson Space Center) lunar regolith simulant measurements (Calla and Rathore 2012) and the Chang'E-5 mission (Su et al. 2022).

Although these studies help us understand the lunar subsurface, it is still challenging to predict the permittivity of future exploration sites. This is because the permittivity is dependent on various parameters such as applied frequency, water content, chemical composition, and temperature (Campbell and Ulrichs 1969; Hansen 1973; Heiken et al. 1991; Jones and Friedman 2000; Shkuratov and Bondarenko 2001; Topp et al. 1980), that is, the permittivity should be treated with the constraints of these parameters. Future GPRs also use a higher frequency band than previous in-situ observations to acquire higher resolution, so it is unclear whether the permittivity at other frequencies can be applied to the analysis of GPRs. In addition, the chemical composition of lunar rocks and regolith has a wide range (e.g., Heiken et al. 1991; Lemelin et al. 2022). Thus, it is not easy to estimate the permittivity at different landing sites from only the measurement of returned samples. Although the measurement of permittivity of simulants is helpful for this purpose, the chemical composition is adjusted to be similar to Apollo samples and the variation has less. Although the effect of temperature on the permittivity is also significant, especially in the low temperature regions such as the permanently shadowed regions, few previous researches have considered the effect in the frequency band for GPR. Calla and Rathore (2012) reported on the temperature dependence of permittivity by measuring the JSC-1A simulant, which is partly very useful to consider the permittivity under the low-temperature environment on the Moon. However, the JSC-1A simulant is manufactured to represent Mare region, not highland and polar region. Thus, the permittivity of highland and polar region at low temperatures has been unclear. Furthermore, the permittivity of water–ice is about 3.1–3.2 (Fujita et al. 2000), which is very close to that of the lunar subsurface. This means that it is unreliable to analyse water–ice existence from the roughly estimated permittivity. To gain useful results for near-future lunar missions, we need to precisely estimate the permittivity at landing sites with various chemical compositions.

In this letter, we focus not on the mixture of lunar simulant, but the typical lunar regolith end-members covering the whole lunar surface of mare, highland, and polar regions (useful for arbitrary mixture permittivity estimations), and report permittivity measurements on different frequencies, which are useful for the GPR data analysis. We simulate the lunar surface/subsurface environment of the polar regions and measure the permittivity with high accuracy in the UHF–SHF band. Knowing the permittivity of several lunar simulants as the end-member of lunar regolith has an advantage to enable us to estimate the bulk permittivity of regolith with an arbitrary composition in the future. Our results highlight the importance of keeping the temperature dependence of various minerals in mind when studying radar data, because other basic lunar regolith materials could be mistaken for water–ice content. The new water–ice hunting lunar missions already on their way to the Moon, working or planned to start in the next years make our results a timely addition to the field.

Experiment methodology

We measure the permittivity of four samples, including rocks and a pure mineral, that typically exist on the Moon (Additional file 1: Fig. S1 and Additional file 3: Table S1): anorthosite, basalt, dunite and ilmenite. Anorthosite, mainly composed of plagioclase accompanying several types of mafic minerals, is distributed widely on the lunar highland and is considered as a representative material for a primitive crust. According to the data from the Kaguya Spectral Profiler measurement, the polar regions can be characterized by a mixture of homogeneous plagioclase (up to 90 wt%) and FeO (<15 wt%) content (Lemelin et al. 2022). Thus, the permittivity of anorthosite is crucial for interpreting the data of the radar observations by LUPEX and Chang'E, while basalt is typically found in Mare regions. Using the permittivity of anorthosite and basalt we can roughly estimate the bulk permittivity in almost all lunar regions. Besides, as mafic materials, we measured the permittivity of dunite (mainly composed of olivine, located in the region where the crust is relatively thin), which exists on the floor of the SPA basin, and its permittivity should be significant for the analysis of the Lunar Penetrating Radar (LPR) data on Chang'E-4 Yutu-2 rover. In addition, the bulk

permittivity of the lunar surface and subsurface could be affected by a small fraction of other materials, especially with high concentrations of Fe and/or Ti (Heiken et al. 1991; Olhoeft and Strangway 1975), and thus, we also measure the permittivity of ilmenite. The chemical composition of the geological samples is measured by X-Ray Fluorescence (XRF) to consider the adequacy of samples for the simulated lunar materials. The measurement is conducted using ZSX Primus II (Rigaku) at 50 kV. Additional file 3: Table S2. shows the chemical composition of each sample. We also checked the modal composition of anorthosite to conduct the point counting method, and confirmed that the anorthosite consistes of mostly Ca-rich plagioclase (92 vol% at most) and with minor pyroxene and olivine, which is consistent with the Apollo sample from highland (Heiken et al. 1991). The bulk composition of basalt is within the chemical composition of the Apollo samples except for TiO_2 and FeO, which may result from the lack of ilmenite. The grain density of each sample is also measured using a 25 mL Gay–Lussac pycnometer. As in the case of the ilmenite, the grain density is the ideal one (Holden 1921).

Sample preparation

The coaxial probe method requires uniformly mixed samples for accurate permittivity measurements, so we crushed the solid samples into fine powders to exclude heterogeneity (Additional file 1: Fig. S1). A few to tens of centimetre-sized samples are first crushed with the hammer and jaw crusher (CR-200B; Marubishi Scientific Instrument Meg. CO., LTD) into smaller than 10 mm, then crushed further with the stamp mill made of stainless steel (ANS-143PS; NITTO KAGAKU CO., LTD). We then sieved the powders with 46 μm with JIS standard sieves. The grain size of ilmenite is about hundreds micrometers, and the basalt is sieved with 500 μm because this sample has a mineral dependence on the particle size and the sieving would exclude some minerals arbitrarily. We then baked the samples at 95 °C for a day or more in the oven to get rid of the water content because the lunar regolith is mostly dry (at the polar regions it is more complex as ice might exist under dry regolith), and the existence of water could affect the bulk permittivity of the samples (Olhoeft and Strangway 1975; Topp et al. 1980). To remove the effect of porosity on the permittivity, which is one of the most effective parameters on the permittivity, we carefully arranged each sample to have the same porosity of 40 %, which is relevant for the top cm–dm layer although at 1 m below the porosity is much smaller. The porosity can change with tapping so we treated the samples carefully, minimising vibrations before the measurement. This preparation makes it possible to measure the permittivity depending on only the difference of materials under the constrained environment.

Permittivity measurement

Various methods are proposed to measure the permittivity (Venkatesh and Raghavan 2005), but coaxial probe method is the most accurate with high reproducibility at the UHF–SHF band. The method utilises the reflection caused by the impedance mismatch between the probe and the samples (Wang et al. 2020). The reflection is measured at a single network port as the S_{11} parameter which describes the ratio of input to output power in an electrical instrument. We used the coaxial probe and cable (85070E Dielectric Probe Kit; Keysight) and the vector network analyzer (VNA; 8753ES S-parameter Network Analyzer; Keysight) (Additional file 2: Fig. S2), with frequency between 1 MHz to 6 GHz in 1601 points (the frequency resolution is ∼3.7 MHz). To make the measurement stable, we warm up the vector network analyzer for 60 minutes before measurements. For the calibration, air, short, and pure water are used, which is the standard method for using the coaxial probe method (Blackham and Pollard 1997). We include the numerical results of the room temperature (20 °C),−20 °C, and −60 °C deep freezer experiments in this Letter as we use these to determine the permittivity of an arbitrary mixture.

Results

To quantify the measurement error of the developed experimental system, we measured the permittivity of air and pure water after calibration, before and after the room temperature experiments. The permittivity values and standard errors of air and pure water measurements are in Additional file 3: Tables S3 and S4 comparing with Barthel et al. (1991). The maximum relative error of air is 2.8 % at 1 GHz and $\leq$ 1.0 % above 2 GHz, while that of pure water is 1.3 % at 1.7 GHz and $\leq$ 0.8 % above 2.05 GHz. As the maximum relative error is more prominent at 1 GHz than at frequencies higher than 2 GHz, we show the measurement results of the permittivity of geological samples between 2 GHz and 6 GHz.

We list the permittivity results of each sample at 20 °C, −20 °C, and −60 °C in Tables 1, 2 and 3. We measured every sample several times, with the probe positioned in various places on the surface of the samples to exclude the effects of the non-uniformity of the powdered samples (see Additional file 2: Fig. S2 in the Appendix for the experimental setup). The permittivity of the samples, with the exception of ilmenite is about 3, which is

Table 1 Permittivity of the samples having 40% porosity at 20 °C

Sample	2 GHz	3 GHz	4 GHz	5 GHz	6 GHz
Anorthosite	3.048 ± 0.044	3.063 ± 0.044	3.091 ± 0.044	3.085 ± 0.044	3.073 ± 0.044
Basalt	3.523 ± 0.034	3.523 ± 0.035	3.558 ± 0.035	3.546 ± 0.034	3.534 ± 0.034
Dunite	3.197 ± 0.037	3.174 ± 0.035	3.213 ± 0.037	3.206 ± 0.037	3.207 ± 0.036
Ilmenite	8.196 ± 0.041	8.041 ± 0.042	7.973 ± 0.049	7.973 ± 0.049	7.732 ± 0.040

The value shows the average of 5 points below and 5 points above each frequency (e.g., the average of the permittivity from 1.984–2.018 GHz in the case of 2 GHz)
In the case of 6 GHz, it is averaged with the 10 points only below the frequency (i.e., the average of the permittivity from 5.966–6.000 GHz)

Table 2 Permittivity of the samples having 40% porosity at −20 °C

Sample	2 GHz	3 GHz	4 GHz	5 GHz	6 GHz
Anorthosite	2.802 ± 0.028	2.805 ± 0.028	2.875 ± 0.028	2.905 ± 0.028	2.922 ± 0.029
Basalt	3.199 ± 0.073	3.218 ± 0.068	3.253 ± 0.073	3.295 ± 0.072	3.313 ± 0.077
Dunite	2.970 ± 0.026	3.002 ± 0.026	3.036 ± 0.026	3.069 ± 0.027	3.085 ± 0.026
Ilmenite	N/A	N/A	N/A	N/A	N/A

The value shows the average of 5 points below and 5 points above each frequency (e.g., the average of the permittivity from 1.984 to 2.018 GHz in the case of 2 GHz)
In the case of 6 GHz, it is averaged with the 10 points only below the frequency (i.e., the average of the permittivity from 5.966 to 6.000 GHz). The permittivity of ilmenite is not measured because the limitation of stabilisation

Table 3 Permittivity of the samples having 40 % porosity at −60 °C

Sample	2 GHz	3 GHz	4 GHz	5 GHz	6 GHz
Anorthosite	2.631 ± 0.029	2.665 ± 0.030	2.690 ± 0.031	2.752 ± 0.031	2.758 ± 0.032
Basalt	2.877 ± 0.050	2.927 ± 0.051	2.945 ± 0.051	3.011 ± 0.053	3.020 ± 0.052
Dunite	2.879 ± 0.029	2.915 ± 0.029	2.951 ± 0.030	3.013 ± 0.031	3.027 ± 0.031
Ilmenite	7.338 ± 0.099	7.288 ± 0.100	7.309 ± 0.101	7.327 ± 0.102	7.287 ± 0.102

The value shows the average of 5 points below and 5 points above each frequency (e.g., the average of the permittivity from 1.984–2.018 GHz in the case of 2 GHz)
In the case of 6 GHz, it is averaged with the 10 points only below the frequency (i.e., the average of the permittivity from 5.966 to 6.000 GHz)

approximately consistent with the Apollo return sample results (Heiken et al. 1991). In the case of ilmenite, the permittivity is higher, about 7–8, which is consistent with previous results of the permittivity being strongly dependent on the $FeO+TiO_2$ content (Heiken et al. 1991).

We found that permittivity displays a strong temperature dependence, which is different for each sample. Comparing the 20 °C and −60 °C results, the permittivity of basalt changes by ~15–18 %, the permittivity of anorthosite changes by ~10–14 % and dunite shows only a ~6–10 % difference. The permittivity of ilmenite also varies by about only ~6–10 %, but the maximum absolute value change in the case of ilmenite is ~0.9, which is larger than in the case of the other samples. The temperature dependence on the permittivity of lunar simulant has been previously reported by Calla and Rathore (2012). They described that the permittivity of JSC-1A at 2.5 GHz is about 4.13 and 4.01 at 30 °C and − 50 °C, respectively, which indicates that the decrease is about 3.0 %. This difference is smaller than our measurement results. The theoretical research, based on the Debye model detailed in Yushkova and Kibardina (2017), reports that the permittivity decrease between 20 °C and −60 °C at 1 GHz is about 13 % (see Fig. 4 in Yushkova and Kibardina 2017). Thus, our result is comparatively similar to the theoretical estimation of the permittivity at temperatures rather than the pervious measurement result of lunar simulant. At lower temperatures, such as 40–80 K (which is a typical temperature in the permanently shadowed regions), theoretical estimation of the permittivity of lunar simulants suggests that the permittivity should not decrease further after reaching a certain temperature (Yushkova and Kibardina 2017). This limit is about 200 K or less in the UHF–SHF band, so our results at −60 °C might be close to the lowest permittivity value (possibly somewhat larger). This should be confirmed by measuring at lower temperatures in the future work.

A simple demonstration of our results with the Looyenga–Landau–Lifshitz equation (which is one of the mixing equations of permittivity) (Looyenga 1965) would be the following: let us assume that 1) a lunar rover equipped

with GPR utilising 4 GHz measured 3.0 permittivity at an anorthositic regolith site (e.g., lunar polar region), and 2) the porosity is 40 % (the relevant for the top cm–dm layer). Using the Looyenga–Landau–Lifshitz equation, the permittivity with 40 % porosity of anorthositic regolith resulting from our measurements, and the permittivity of 3.1 for water–ice (Fujita et al. 2000), we can estimate the water–ice content as 4.4 wt% at −20 °C and 11.2 wt% at −60 °C. This means that because the permittivity of rock fraction is different at the two temperatures, the water–ice content estimated from the permittivity of 3.0 is different (even though the permittivity measured at the regolith site is the same). The difference between the two estimated water–ice contents indicates that for an accurate water–ice abundance estimation temperature information is also required, to consider the temperature dependent permittivity. In addition to the temperature information, the materials' variation is also required: our results show how this temperature dependence is different for each geological sample; thus, the permittivity of lunar regolith should be estimated in the future while considering these variations. For example, if the content of ilmenite, which is one of the largest permittivity in the regolith, is not considered accurately, the higher permittivity could falsely suggest water–ice content from radar measurement. We highlight the importance to take the possibility that the measured permittivity could be a consequence of ilmenite-content into consideration. In addition, the observation of the porosity of regolith is difficult with existing method in-situ. Thus, it is required to develop the method to obtain the porosity and water–ice content with the consideration of the chemical composition of the lunar regolith at an arbitrary site. To aid this, we are developing a method to quantify the water–ice content focusing on the different temperature dependencies on the permittivity of rocks, minerals, and water–ice (Kobayashi et al., in prep.).

Most of the previous works analysing GPR data of the Moon relies on the relationship between the permittivity of the Apollo samples and bulk density (Heiken et al. 1991; Olhoeft and Strangway 1975):

$$\epsilon = 1.919^{\varrho} \tag{1}$$

where ϱ is the bulk density in g/cm^3. This empirical formula (Eq. 1) is useful as a rough average estimation of the permittivity of the lunar subsurface; however, since it was determined by fitting the permittivity measurements of the Apollo samples under various conditions, it is less accurate at specific locations. In addition, because each material showed a different temperature dependence, it is difficult to estimate the permittivity of the lunar regolith at low temperatures based on Eq. 1. We calculate the permittivity based on Eq. 1 and the density of the samples used in the measurements.

While the permittivity at 20 °C and −20 °C are both larger than the value coming from Eq. 1, the permittivity at −60 °C is lower (Fig. 1). This indicates that GPR analysis using Eq. 1. cannot consider the temperature dependence on the permittivity, which could lead to the wrong estimation of the subsurface structure and even of the existence of water–ice. Furthermore, it is unclear whether Eq. 1 can be applied to the analysis using GPRs because of the difference in frequency range, since the equation is acquired by fitting the data measured at a lower frequency (typically 10–450 MHz). Our results in the UHF–SHF band show that while the permittivity is slightly affected by the frequency, the variation is considerably larger in the case of ilmenite (Fig. 1), which is consistent with previous studies (e.g., Stillman and Olhoeft 2008). Overall, our results indicate that though the permittivity changes with temperature change, the variation ranges widely and should be treated carefully to consider the materials present at the radar-scanned location; which makes the subsurface structure and even water–ice existence estimations possible in future missions.

Conclusions

To appropriately evaluate GPR data from previous and future lunar missions, we need to take the variations in chemical composition, temperature conditions, and porosities of the lunar regolith into consideration. We evaluated these effects individually from laboratory measurements: first, we prepared lunar representative materials, based on chemical studies of the Apollo return samples, meteorite studies and remote-sensing observations. We determined the 4 end-member rocks and minerals for radar observations, such as anorthosite, basalt, dunite, and ilmenite. We developed a system to measure the permittivity of powdered samples in the 2–6 GHz frequency range with high precision (less than 1% relative error). We prepared powdered samples of the 4 identified end-members and measured their permittivity at different temperatures (20 °C, −20 °C, and −60 °C).

We found that the permittivity of lunar simulant materials has a complex dependency on several parameters. The content of ilmenite increases the bulk permittivity of the lunar regolith, which is also strongly dependent on temperature. The permittivity decreases at lower temperatures, typically of the geological samples by 6–18% between −60 °C and 20 °C. Previous works did not accurately consider the temperature dependent differences of permittivity when estimating the permittivity of the lunar subsurface, thus our results fill an important knowledge gap, while being consistent with former research (e.g.,

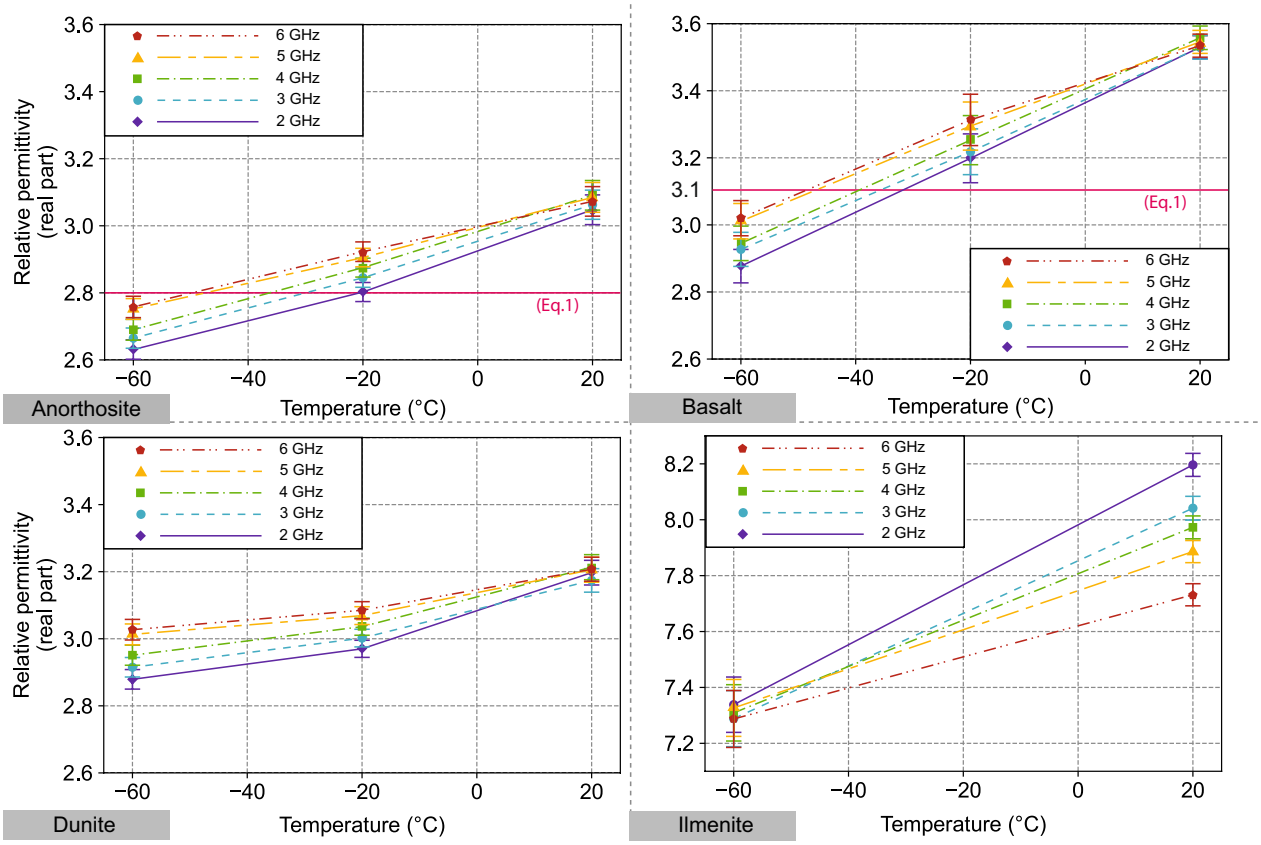

Fig. 1 Temperature dependence of the permittivity. **a** Anorthosite, **b** Basalt, **c** Dunite, and **d** Ilmenite. The circular points are the average of 10 points below and above each frequency (e.g., the average of the permittivity from 1.984–2.018 GHz in the case of 2 GHz). In the case of 6 GHz, it is averaged with the 10 points only below the frequency (i.e., the average of the permittivity from 5.966 to 6.000 GHz). The error bar shows the standard error. The colour shows the frequency (dark purple: 2 GHz, light blue: 3 GHz, green: 4 GHz, orange: 5 GHz, and dark red: 6 GHz), while the horizontal line shows the calculation result based on Eq. 1. in magenta, where appropriate. The calculation result is only shown in the case of the anorthosite and basalt, because Eq. 1 was derived from the Apollo sample and the dunite and ilmenite are minor components in the Apollo sample

Yushkova and Kibardina , 2017). While they reported the temperature dependence of the permittivity of lunar simulants, our paper reported first on the difference between temperature dependence on each lunar simulant representing lunar regolith end-members. Thus, we should consider the effect on the permittivity carefully when discussing about the existence of water–ice with radar observations at the cold polar lunar regions.

While we reported that the permittivity of lunar materials depends on temperature, this is not true for water–ice (Fujita et al. 2000). This implies that by measuring lunar regolith permittivity at different temperatures (different local times), the water–ice content could be calculated from permittivity variations (Kobayashi et al., in prep). Thus we propose that using the results from our future new method the existence of even small amounts of water–ice could be detected by radar data collected at different temperatures.

Abbreviations

GPR	Ground-penetrating radar
EM	Electromagnetic
JSC	Johnson Space Center
UHF–SHF	Ultra high frequency–super high frequency
LPR	Lunar Penetrating Radar
XRF	X-Ray fluorescence
VNA	Vector Network Analyzer
SPA	South Pole-Aitken

Supplementary Information

The online version contains supplementary material available at https://doi.org/10.1186/s40623-022-01757-5.

Additional file 1: Figure S1. Geological samples for our permittivity measurements. a) Anorthosite, b)Basalt, c) Dunite and d) Ilmenite

Additional file 2: Figure S2. Experimental setup. a) The Vector Network Analyzer (VNA; 8753ES) used for our measurement. b) Appearance of our measurement system. The coaxial probe is set inside the deep freezer (up to -60 °C). To avoid the temperature change inside, the lid is closed during each measurement. c) Inside of the deep freezer. On the floor, a lab jack is

set to touch the samples with probe. The coaxial probe is covered with an aluminium foil to prevent frost forming on the surface. d) Enlarged view of the sample and coaxial probe. To exclude the chemical and mineral heterogeneity on the surface of samples, the measurement was conducted by setting the probe to different places on the surface of the samples.

Additional file 3: Table S1. Geological samples for our permittivity measurements. Anorthosite and dunite, which is aquiredas solid pieces, are crushed into microns' size and sieved with 46 μm for stacking to the coaxial probe.The basalt has the mineral dependence on the particle size, so the sample having a broad particle sizeis used for the measurement. The grain density of ilmenite is referred from Holden [1921]. **Table S2.** Chemical composition of samples measured by XRF. The chemical composition of ilmenite isthe ideal one calculated based on the chemical formula. **Table S3.** Measured permittivity, standard error, and maximum relative error of air. Higher than 2 GHz,the maximum relative error is less than 1.0 %. **Table S4.** Measured permittivity, standard error, and maximum relative error of pure water comparedwith Barthel et al. (1991). Higher than 2.05 GHz, the maximum relative error is less than 1.0 %.

Acknowledgements
We are grateful to Dr. Kazutaka Yasukawa for support on XRF measurements. This work is supported in part by the Ministry of Internal Affairs and Communications of Japanese Government Reiwa 4-0155-0099, by JAXA's Feasibility Study 2022, by the University of Tokyo's International Graduate Program for Excellence in Earth-Space Science (IGPEES), and the 164800 MÁEÖ bilateral scholarship of the Tempus Public Foundation.

Author contributions
MK and HM conceived the idea of the study. MK and TN developed the measurement system. MK, TN, and TT contributed to the sample preparation. MK conducted the measurement. MK, HM, and BDP contributed to the interpretation of the results. MK, HM, and BDP drafted the original manuscript. HM supervised the conduct of this study. All authors read and approved the final manuscript.

Funding
This work is supported in part by the Ministry of Internal Affairs and Communications of Japanese Government Reiwa 4-0155-0099, by JAXA's Feasibility Study 2022, by the University of Tokyo's International Graduate Program for Excellence in Earth-Space Science (IGPEES), and the 164800 MÁEÖ bilateral scholarship of the Tempus Public Foundation.

Availability of data and materials
The datasets used and/or analyzed during the current study are available from the corresponding author on reasonable request.

Declarations

Competing interests
The authors declare that they have no competing interest.

Author details
[1]Department of Earth and Planetary Science, School of Science, University of Tokyo, Tokyo, Japan. [2]Department of Systems Innovation, School of Engineering, University of Tokyo, Tokyo, Japan. [3]Department of Earth and Planetary Science, School of Science, University of Tokyo, Tokyo, Japan. [4]Konkoly Observatory, Research Centre for Astronomy and Earth Sciences, Budapest, Hungary. [5]CSFK, MTA Centre of Excellence, Budapest, Hungary. [6]Department of Applied Science, Faculty of Science, Okayama University of Science, Okayama, Japan. [7]Department of Systems Innovations, School of Engineering, University of Tokyo, Tokyo, Japan.

Received: 29 September 2022 Accepted: 20 December 2022
Published online: 19 January 2023

References

Arnold JR (1979) Ice in the lunar polar regions. J Geophys Res Solid Earth 84:5659–5668
Barthel J, Bachhuber K, Buchner R, Hetzenauer H, Kleebauer M (1991) A computer-controlled system of transmission lines for the determination of the complex permittivity of lossy liquids between 8.5 and 90 ghz. Ber Bunsenges Phys Chem. https://doi.org/10.1002/bbpc.19910950802
Blackham D, Pollard R (1997) An improved technique for permittivity measurements using a coaxial probe. IEEE Trans Instrum Meas 46(5):1093–1099
Boazman S, Kereszturi A, Heather D, Sefton-Nash E, Orgel C, Tomka R, Houdou B, Lefort X (2022) Analysis of the Lunar South Polar Region for PROSPECT, NASA/CLPS. Eur Planet Sci Congr. https://doi.org/10.5194/epsc2022-530
Calla OPN, Rathore IS (2012) Study of complex dielectric properties of lunar simulants and comparison with Apollo samples at microwave frequencies. Adv Space Res 50(12):1607–1614
Campbell MJ, Ulrichs J (1969) Electrical properties of rocks and their significance for lunar radar observations. J Geophys Res 74(25):5867–5881
Chung DH, Westphal WB (1973) Dielectric spectra of Apollo 15 and 16 lunar solid samples. Lunar Planet Sci Conf Proc 4:3077
Colaprete A, Andrews D, Bluethmann W, Elphic RC, Bussey B, Trimble J, Zacny K, Captain JE (2019) An Overview of the Volatiles Investigating Polar Exploration Rover (VIPER) Mission. AGU Fall Meeting Abstracts. 2019:P34B-03
Colaprete A, Schultz P, Heldmann J, Wooden D, Shirley M, Ennico K, Hermalyn B, Marshall W, Ricco A, Elphic RC, Goldstein D, Summy D, Bart GD, Asphaug E, Korycansky D, Landis D, Sollitt L (2010) Detection of water in the LCROSS ejecta plume. Science 330(6003):463
Dong Z, Fang G, Ji Y, Gao Y, Wu C, Zhang X (2017) Parameters and structure of lunar regolith in Chang'E-3 landing area from lunar penetrating radar (LPR) data. Icarus 282:40–46
Dong Z, Fang G, Zhou B, Zhao D, Gao Y, Ji Y (2021) Properties of Lunar Regolith on the Moon's Farside Unveiled by Chang'E-4 Lunar Penetrating Radar. J Geophys Res 126(6):e06564
Feldman WC, Maurice S, Binder AB, Barraclough BL, Elphic RC, Lawrence DJ (1998) Fluxes of fast and epithermal neutrons from Lunar prospector: evidence for water ice at the Lunar poles. Science 281:1496
Fisher EA, Lucey PG, Lemelin M, Greenhagen BT, Siegler MA, Mazarico E, Aharonson O, Williams J-P, Hayne PO, Neumann GA, Paige DA, Smith DE, Zuber MT (2017) Evidence for surface water ice in the lunar polar regions using reflectance measurements from the Lunar Orbiter Laser Altimeter and temperature measurements from the Diviner Lunar Radiometer Experiment. Icarus 292:74–85
Frisillo AL, Olhoeft GR, Strangway DW (1975) Effects of vertical stress, temperature and density on the dielectric properties of lunar samples 72441,12, 15301,38 and a terrestrial basalt. Earth Planet Sci Lett 24(3):345–356
Fujita S, Matsuoka T, Ishida T, Matsuoka K, Mae S (2000) A summary of the complex dielectric permittivity of ice in the megahertz range and its applications for radar sounding of polar ice sheets. In: Fujita S (ed) Physics of ice core records. Hokkaido University Press, Hokkaido, pp 185–212
Gold T, Bilson E, Baron RL (1976) Electrical properties of Apollo 17 rock and soil samples and a summary of the electrical properties of lunar material at 450 MHz frequency. Lunar Planet Sci Conf Proc 3:2593–2603
Hansen W (1973) The dielectric properties of selected basalts. Geophysics 38(1):135
Hayne PO, Hendrix A, Sefton-Nash E, Siegler MA, Lucey PG, Retherford KD, Williams J-P, Greenhagen BT, Paige DA (2015) Evidence for exposed water ice in the Moon's south polar regions from Lunar reconnaissance orbiter ultraviolet albedo and temperature measurements. Icarus 255:58–69
Heiken GH, Vaniman DT, French BM (1991) Lunar sourcebook, a user's guide to the moon
Holden EF (1921) Specific gravity and composition in iron rutile. Am Mineral J Earth Planet Mater 6(6):100–103
Hoshino T, Wakabayashi S, Ohtake M, Karouji Y, Hayashi T, Morimoto H, Shiraishi H, Shimada T, Hashimoto T, Inoue H, Hirasawa R, Shirasawa Y, Mizuno H, Kanamori H (2020) Lunar polar exploration mission for water prospection–JAXA's current status of joint study with ISRO. Acta Astronaut 176:52–58

Ishiyama K, Kumamoto A, Ono T, Yamaguchi Y, Haruyama J, Ohtake M, Katoh Y, Terada N, Oshigami S (2013) Estimation of the permittivity and porosity of the lunar uppermost basalt layer based on observations of impact craters by SELENE. J Geophy Res 118(7):1453–1467
Jones SB, Friedman SP (2000) Particle shape effects on the effective permittivity of anisotropic or isotropic media consisting of aligned or randomly oriented ellipsoidal particles. Water Resour Res 36(10):2821–2833
Kereszturi A (2020) Polar ice on the moon. Springer International Publishing, Cham, pp 1–9. https://doi.org/10.1007/978-3-319-05546-6_216-1
Lawrence DJ, Feldman WC, Elphic RC, Hagerty JJ, Maurice S, McKinney GW, Prettyman TH (2006) Improved modeling of Lunar Prospector neutron spectrometer data: implications for hydrogen deposits at the lunar poles. J Geophys Res 111(E8):E08001
Lemelin M, Lucey PG, Camon A (2022) Compositional Maps of the Lunar polar regions derived from the Kaguya spectral profiler and the Lunar orbiter laser altimeter data. Planet Sci J 3(3):63
Li C, Su Y, Pettinelli E, Xing S, Ding C, Liu J, Ren X, Lauro SE, Soldovieri F, Zeng X, Gao X, Chen W, Dai S, Liu D, Zhang G, Zuo W, Wen W, Zhang Z, Zhang X, Zhang H (2020) The Moon's farside shallow subsurface structure unveiled by Chang'E-4 Lunar Penetrating Radar. Sci Adv 6(9):eaay6898
Li S, Lucey PG, Milliken RE, Hayne PO, Fisher E, Williams J-P, Hurley DM, Elphic RC (2018) Direct evidence of surface exposed water ice in the lunar polar regions. Proc Natl Acad Sci 115(36):8907–8912
Looyenga H (1965) Dielectric constants of heterogeneous mixtures. Physica 31(3):401–406
Martinez A, Byrnes AP (2001) Modeling dielectric-constant values of geologic materials: an aid to ground-penetrating radar data collection and interpretation. Curr Res Earth Sci. https://doi.org/10.17161/cres.v0i247.11831
Miller RS, Nerurkar G, Lawrence DJ (2012) Enhanced hydrogen at the lunar poles: New insights from the detection of epithermal and fast neutron signatures. J Geophys Res 117(E11):E11007
Nozette S, Lichtenberg CL, Spudis P, Bonner R, Ort W, Malaret E, Robinson M, Shoemaker EM (1996) The Clementine Bistatic Radar experiment. Science 274(5292):1495–1498
Olhoeft GR, Strangway DW (1975) Dielectric properties of the first 100 meters of the Moon. Earth Planet Sci Lett 24(3):394–404
Pieters CM, Goswami JN, Clark RN, Annadurai M, Boardman J, Buratti B, Combe JP, Dyar MD, Green R, Head JW, Hibbitts C, Hicks M, Isaacson P, Klima R, Kramer G, Kumar S, Livo E, Lundeen S, Malaret E, McCord T, Mustard J, Nettles J, Petro N, Runyon C, Staid M, Sunshine J, Taylor LA, Tompkins S, Varanasi P (2009) Character and Spatial Distribution of OH/H_2O on the Surface of the Moon Seen by M^3 on Chandrayaan-1. Science 326(5952):568
Sanin AB, Mitrofanov IG, Litvak ML, Bakhtin BN, Bodnarik JG, Boynton WV, Chin G, Evans LG, Harshman K, Fedosov F, Golovin DV, Kozyrev AS, Livengood TA, Malakhov AV, McClanahan TP, Mokrousov MI, Starr RD, Sagdeev RZ, Tret'yakov VI, Vostrukhin AA (2017) Hydrogen distribution in the lunar polar regions. Icarus 283:20–30
Shkuratov YG, Bondarenko NV (2001) Regolith layer thickness mapping of the moon by radar and optical data. Icarus 149(2):329–338
Spudis PD, Bussey DBJ, Baloga SM, Cahill JTS, Glaze LS, Patterson GW, Raney RK, Thompson TW, Thomson BJ, Ustinov EA (2013) Evidence for water ice on the moon: results for anomalous polar craters from the LRO Mini-RF imaging radar. J Geophys Res 118(10):2016–2029
Stillman D, Olhoeft G (2008) Frequency and temperature dependence in electromagnetic properties of Martian analog minerals. J Geophys Res 113(E9):E09005
Su Y, Wang R, Deng X, Zhang Z, Zhou J, Xiao Z, Ding C, Li Y, Dai S, Ren X, Zeng X, Gao X, Liu J, Liu D, Liu B, Zhou B, Fang G, Li C (2022) Hyperfine structure of Regolith Unveiled by Chang'E-5 Lunar Regolith penetrating radar. IEEE Trans Geosci Remote Sens 60:3148200
Topp GC, Davis JL, Annan AP (1980) Electromagnetic determination of soil water content: measurements in coaxial transmission lines. Water Resour Res 16(3):574–582
Venkatesh M, Raghavan V (2005) An overview of dielectric properties measuring techniques. Can Biosyst Eng 47:15–30
Wang J, Lim EG, Leach MP, Wang Z, Man KL (2020) Open-ended coaxial cable selection for measurement of liquid dielectric properties via the reflection method. Math Prob Eng 2020:1–8
Watson K, Murray B, Brown H (1961) On the possible presence of ice on the moon. J Geophys Res 66(5):1598–1600
Xiao L, Zhu P, Fang G, Xiao Z, Zou Y, Zhao J, Zhao N, Yuan Y, Qiao L, Zhang X, Zhang H, Wang J, Huang J, Huang Q, He Q, Zhou B, Ji Y, Zhang Q, Shen S, Li Y, Gao Y (2015) A young multilayered terrane of the northern Mare Imbrium revealed by Chang'E-3 mission. Science 347(6227):1226–1229
Yushkova O, Kibardina I (2017) Dielectric properties of lunar surface. Solar Syst Res 51(2):121–126
Zhang L, Li J, Zeng Z, Xu Y, Liu C, Chen S (2020) Stratigraphy of the Von Kármán Crater Based on Chang'E-4 Lunar Penetrating Radar Data. Geophys Res Lett 47(15):e88680
Zuber MT, Head JW, Smith DE, Neumann GA, Mazarico E, Torrence MH, Aharonson O, Tye AR, Fassett CI, Rosenburg MA, Melosh HJ (2012) Constraints on the volatile distribution within Shackleton crater at the lunar south pole. Nature 486(7403):378–381

Publisher's Note